Available online at www.sciencedirect.com
ScienceDirect
International Journal of Heat and Mass Transfer 50 (2007) 2905–2911
International Journal of HEAT and MASS TRANSFER
www.elsevier.com/locate/ijhmt

Evaporation heat transfer characteristics of a grooved heat pipe with micro-trapezoidal grooves

A.J. Jiao, H.B. Ma *, J.K. Critser

Department of Mechanical and Aerospace Engineering, University of Missouri, Columbia, MO 65211, USA

Received 22 June 2006; received in revised form 6 January 2007
Available online 21 March 2007

Abstract

A detailed mathematical model predicting the effect of contact angle on the meniscus radius, thin film profile and heat flux distribution occurring in the micro-trapezoidal grooves of a heat pipe has been presented. The model can be used to determine the maximum evaporating heat transfer rate in the evaporator including the effects of disjoining pressure and surface tension. The equation of meniscus radii calculation in the evaporator at given heat load based on the liquid wicks configuration has been put forward. The numerical results show that while the capillary limitation governs the maximum heat transport capability in a grooved heat pipe, the thin film evaporation determines the effective thermal conductivity in a grooved heat pipe. The ratio of the heat transfer through the thin film region to the total heat transfer through the wall to the vapor phase decreases when the contact angle increases. The superheat effects on the heat flux distribution in the thin film region also have been conducted and the results show that the disjoining pressure plays an important role in this region. The current investigation will result in a better understanding of thin film evaporation and its effect on the effective thermal conductivity in a grooved heat pipe.

Keywords: Heat pipe; Thin film evaporation; Effective thermal conductivity

1. Introduction

Many electronic systems often generate very high heat flux, and heat generated must be dissipated in order to keep temperature distribution uniformity, maintain its operating temperature limit and peak performance. When the heat pipe technology is used as a cooling strategy for those modern systems, the further increase of the effective thermal conductivity of the heat pipe is the key for the high-heat flux applications. As a high heat flux is added on the evaporating section of the heat pipe, the thin film evaporation heat transfer plays an important role to keep its operation. A better understanding of the heat transport mechanisms in the thin film region will directly help the designs of highly efficient heat pipes and advanced thermal management systems.

A number of previous investigations [1–4] have been conducted on the thin film evaporation and heat transport occurring in micro-grooves, and indicate that most of the heat is transferred through the region where the thickness of the liquid layer is extremely small. Based on the heat transfer rate, the liquid film around this thin film region is often divided into three regions, namely, the equilibrium non-evaporating film region, evaporating film region, and meniscus region. In the evaporating film region, the disjoining pressure plays key role and affect the interface temperature and heat transfer rate through the thin film. Ma and Peterson [5] found that the evaporating heat transfer coefficient through the thin film region depends on the meniscus radius and the superheat. Previous investigations [6,7] show that when the heat flux level added on the thin film region increases, the contact angle increases resulting in a

* Corresponding author. Tel.: +1 573 884 5944; fax: +1 573 884 5090.
E-mail address: mah@missouri.edu (H.B. Ma).

0017-9310/$ - see front matter © 2007 Elsevier Ltd. All rights reserved.
doi:10.1016/j.ijheatmasstransfer.2007.01.009

Nomenclature

A	Hamaker constant, J
a	constant in Eqs. (4) and (5)
b	constant in Eqs. (4) and (5)
d	half width of wick's top wall in Fig. 1, m
h	height of groove wall, m
h_{fg}	latent heat of vaporization, kJ/kg
h_t	height defined in Fig. 1, m
k	conductivity, W/m K
L	length of evaporator, m
N	number of grooves
p	pressure, N/m^2
p_d	disjoining pressure, N/m^2
Q	heat transfer, W
q	heat flux, W/m^2
R	gas constant, J/kg K
$R_{30,60}$	radius at $\alpha = 30°$ or 60°, m
r	radius, m
s	coordinate, m
T	temperature, K
W	width, m
x	coordinate, m
y	coordinate, m
z	coordinate, m

Greek symbols

α	contact angle, °
β	angle defined in Fig. 1, °
δ	film thickness, m
δ_0	non-evaporating film thickness, m
η	coordinate, m
θ	angle defined in Fig. 1, °
ρ	density, kg/m^3
σ	surface tension, N/m

Subscripts

B–B	B–B thin film region in Fig. 1
C–C	C–C thin film region in Fig. 1
D–D	D–D thin film region in Fig. 1
e	evaporating
g	gas
l	liquid
lv	liquid–vapor interface
men	meniscus
micro	micro-region
macro	macro-region
sat	saturated
th	thickness
tot	total
v	vapor
w	wall
(z)	z coordinate

decrease of the evaporating heat transfer coefficient, which presents a limitation of heat transport capability in a high heat flux heat pipe [8]. Recently, Jiao et al. [9,10] developed a model focusing on the curved surface effect on the thin film profiles and heat flux distributions in the evaporator of a flat heat pipe.

In the design of heat pipe, a number of heat transfer limitations [11–18] should be taken into consideration. Those limitations determine the maximum heat transport occurring in a heat pipe. In order to meet the new requirements, however, it is necessary to further increase the effective thermal conductivity of a heat pipe. The primary thermal resistances in a grooved heat pipe, for example, are from the evaporating thin film and the condensation heat transfer. As indicated above, when the heat flux is high, the increase of the contact angle in an individual evaporating thin film will increase the thermal resistance and directly affect the total effective thermal conductivity. In current investigation, a detailed mathematical model predicting the effect of the thin film region on the evaporating heat transfer in trapezoidal grooves of a grooved heat pipe has been developed in order to find the maximum evaporating heat transport capacity through the thin film region.

2. Meniscus radius and thin film region evaporation heat transfer

When heat is added on the evaporating section of a grooved heat pipe, the heat will transfer through solid regions of groove wall and reach the working fluid. For the groove configuration of a heat pipe shown in Fig. 1, most of the heat will transfer through thin film regions. When the heat load is low, there exist two thin film regions, i.e., C–C, D–D zones, and due to the groove symmetry, the C–C thin film region is the same as the D–D thin film region. But when the heat load reaches the maximum heat load, in which the thin film thickness of point B (δ_B) is equal to δ_0, a new thin film region B–B [4,9] will be formed. Because there is no vapor-solid interface in the B–B thin film region, the contact angle in this region should be equal to zero. If the heat load continues increase, the thin film region B–B will rupture and divide into two thin film regions, in which the total length of the thin film regions will be shorter than that of region B–B due to the contact angle effect. Therefore, the heat transfer performances of heat pipe will become worse and directly result in the temperature difference increase dramatically as the heat load continuously increases. The heat load at $\delta_B = \delta_0$ is the

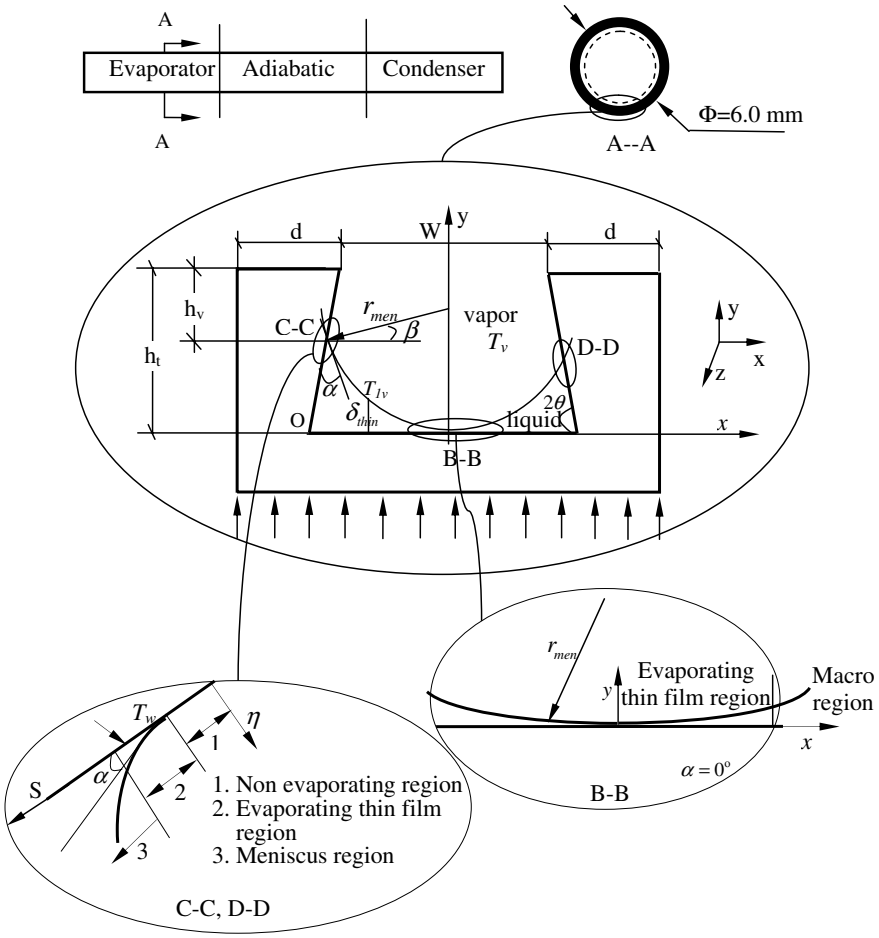

Fig. 1. Schematic of tube heat pipe with micro-trapezoidal liquid wicks configuration.

maximum heat transport capacity of the heat pipe, which is the focus in the current investigation herein. For the thin film evaporation heat transfer, the liquid–vapor interface temperatures on those thin film regions can be depicted by the Clausius–Clapeyron equation:

$$\left(\frac{dp}{dT}\right)_{sat} = \frac{h_{fg}}{T_{sat}[(1/\rho_v) - (1/\rho_l)]} \tag{1}$$

Integrating from the saturated temperature T_{sat} to the interface temperature T_{lv} results in a relationship between the interface temperature and the saturated vapor temperature, i.e.,

$$T_{lv} = T_v[1 + (\Delta p/\rho_v h_{fg})] \tag{2}$$

where Δp can be found from

$$\Delta p = \sigma/r_{(z)} + p_d \tag{3}$$

where the second term, p_d, in Eq. (3) can be estimated by $p_d = -A/\delta^3$ for nonpolar liquids and $p_d = -A/\delta^3 \ln(\delta/\bar{\delta}_0)$ for polar liquids. Because the Hamaker constant A and the reference length $\bar{\delta}_0$ both depend on the solid–liquid properties, it is difficult to accurately determine these values for polar liquids such as water. To overcome this difficulty, the relationship developed by Holm and Goplen [1], i.e.,

$$p_d = \rho_l R_g T_{\delta,v} \ln(a\delta^b) \tag{4}$$

was utilized, where, $a = 1.5787, b = 0.0243$. In the non-evaporating film region, as shown in Fig. 1, the curvature effect can be neglected due to the absence of vaporization. The interface temperature at this region will be equal to the wall temperature due to the interface thermal resistance. Substituting Eqs. (3) and (4) into Eq. (2), the film thickness in this region can be obtained as

$$\delta_0 = \exp\{[(T_w/T_v - 1)(h_{fg}/RT_w) - \ln a]/b\} \tag{5}$$

Based on the contact angle α and dimensions shown in Fig. 1, the meniscus radius, $r_{(z)}$ can be written as

$$r_{(z)} = \frac{W/2 + (h_t - \delta_y)ctg2\vartheta}{\cos\beta + (1 - \sin\beta)ctg2\vartheta} \tag{6}$$

where

$$\beta = \alpha - \left(\frac{\pi}{2} - 2\vartheta\right) \tag{7}$$

$$h_v = h_t - [\delta_y + r_{(z)}(1 - \sin\beta)] \tag{8}$$

When the Bond number is very small, the meniscus radius shown in Eq. (6) only depends on the contact angle, the

thickness of non-evaporating δ_0, and the groove configuration. Based on the geometry dimensions of the trapezoidal shape and the definition of contact angle, the film thickness for both the C–C and D–D regions can be calculated by:

$$\delta_{\text{C–C}} = \delta_{\text{D–D}} = \frac{W}{2} + ctg2\vartheta(h_t - y) - \sqrt{r^2 - [y - (r_{(z)} - \delta_0)]^2} \tag{9}$$

where

$$y = r_{(z)}(1 - \sin\beta) + \delta_0$$
$$\delta_0 \leqslant y \leqslant r_{(z)}[1 - \sin\beta] + \delta_0 \tag{10}$$
$$\delta = \delta_0, \quad r_0 \to \infty, \quad T_{\delta,v} = T_w; \text{ at } s = 0$$

The film thickness variation for the B–B region can be found as

$$\delta_{\text{B–B}} = (r_{(z)} + \delta_0) - \sqrt{r_{(z)}^2 - x^2} \tag{11}$$

where

$$-r_{(z)}\cos\beta \leqslant x \leqslant r_{(z)}\cos\beta$$
$$\delta = \delta_0, \; r_0 \to \infty, \tag{12}$$
$$T_{\delta,v} = T_w, \text{ at } x = 0$$

Heat transfer through the thin film region can be considered as one-dimensional heat conduction. Based on this assumption, the heat flux and total heat transfer through three thin film regions can be calculated by

$$q = k\frac{\Delta T}{\delta} = k\frac{T_w - T_{lv}}{\delta} \tag{13}$$

$$Q_{\text{Micro}} = 2N\left[\int_0^{L_{\text{BE}}} k\frac{T_w - T_{lv}}{\delta_{\text{B–B}}}L_e\,dx + \int_0^{s} k\frac{T_w - T_{lv}}{\delta_\eta}L_e\,ds\right] \tag{14}$$

The second term on the right side of Eq. (14) can be expressed by:

$$-\int_{r_{(z)}[1+\cos(2\vartheta+\alpha)]+\delta_0}^{y} k\frac{T_w - T_{lv}}{\delta_{\text{C–C}}\sin 2\vartheta}L_e\,dy \tag{15}$$

3. Heat transfer through macro-region

Because the groove dimension as shown in Fig. 1 is in a range of 0.1–0.3 mm and the Bond is much less than 1, the temperature distribution in the macro-liquid film region can be described by the two-dimensional, steady-state heat conduction equation,

$$\frac{\partial^2 T}{\partial x^2} + \frac{\partial^2 T}{\partial y^2} = 0 \tag{16}$$

Although the geometry is not regular, the solution for Eq. (16) can be readily obtained by the FLUENT software, and the total heat transfer through the macro-region can be easily obtained. In this region, the effect of disjoining pressure on the interface temperature can be neglected. The interface temperature can be determined by

$$T_{lv} = T_v\left(1 + \frac{\sigma}{r_{(z)}\rho_v h_{fg}}\right) \tag{17}$$

A number of grid numbers have been employed in order to obtain the grid-independent solutions, and finer grids near the evaporating thin film region were used. Using Eq. (17) for the liquid–vapor interface temperature, the heat transport Q_{macro} through the macro-region of liquid for a given superheat can be calculated. The total heat transport from the solid wall to the liquid can be determined by

$$Q_{\text{tot}} = Q_{\text{macro}} + Q_{\text{micro}} \tag{18}$$

where, Q_{micro} can be calculated by Eq. (14) for a given superheat. During the iterative calculation, when the error is less than 0.1 W, the calculation is considered as the converged results.

4. Results and discussion

The disjoining pressure and interface curvature significantly affect the film thickness variation, interface temperature, and heat flux distribution. In order to better illustrate effects on the meniscus radius, heat flux distribution and heat transport capacity, a trapezoid groove, similar to the one shown in Fig. 1, with dimensions of $W = 0.000262$ m, $h_t = 0.000195$ m, $L = 0.03$ m, 2ϑ=75.8°, and a groove number of 60, was considered. The thermophysical properties of copper and pure saturated water at 60 °C are utilized in the current investigation.

Fig. 2 illustrates the contact angle effect on the meniscus radius including the superheat effect on the non-evaporating film thickness. As shown, the meniscus radius increase nonlinearly as the contact angle increases. For example, when the contact angle changes from $\alpha = 0°$ to $\alpha = 30°$, the radius change slowly and the ratio of the meniscus radius at $\alpha = 30°$ to the one at $\alpha = 0°$ is equal to 1.12, while the ratio of the meniscus radius at $\alpha = 90°$ to the one $\alpha = 60°$ is 3.07. It shows that when the contact angle is less

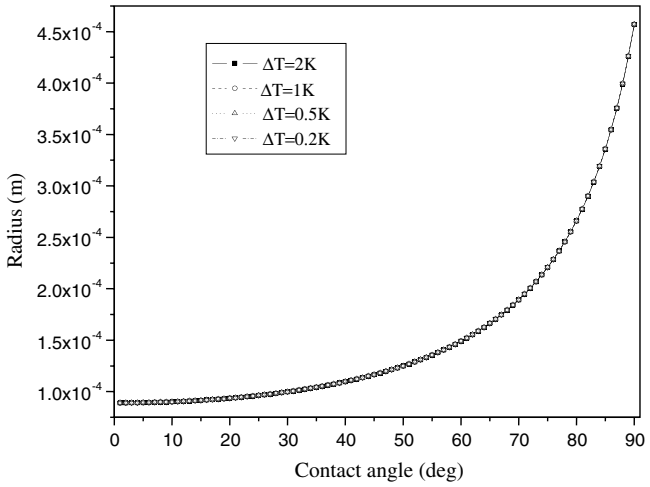

Fig. 2. Meniscus radii versus contact angle.

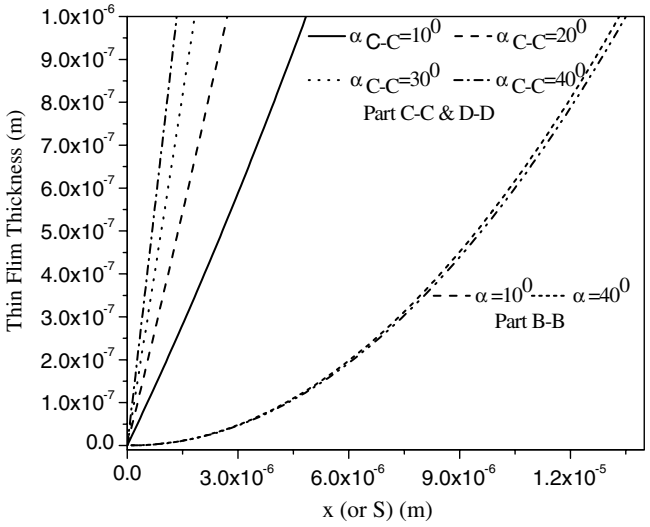

Fig. 3. Contact angle effect on liquid film profiles.

than 30°, the further decrease of the contact angle will not significantly further reduce the meniscus radius.

Fig. 3 shows the contact angle effect on the thin film profiles in both the C–C (or D–D) and B–B regions. As shown, the thin film thickness profile in the C–C (or D–D) region largely depend on the contact angle, while the thin film profile in the B–B region is almost unchanged as the contact angle varies from 10° to 40°. If the cut-off film thickness for the thin film region is $\delta = 1$ μm, for example, the thin film region length decreases from 13.5 μm to 13.4 μm for the B–B region as the contact angle increases from $\alpha = 10°$ to 40°. When the contact angle further increases, however, the thin film profile for the C–C (or D–D) region varies very sharply. With the same cut-off film thickness of $\delta = 1$ μm for the thin film region, the thin film length decreases from 4.8 μm to 1.33 μm as the contact angle increases from $\alpha = 10°$ to 40°. As shown in Fig. 3, the thin film region length of the B–B region is about 2.8–10 times of the one in the C–C region.

Once the thin film profile is given, the heat flux distribution through the thin film regions shown in Fig. 4 can be obtained. As the interface temperature at the liquid–vapor interface varies from $T_{lv} = T_w$ at the non-evaporating film region to $T_{lv} = T_v[1 + \sigma/(r_{(z)}\rho_v h_{fg})]$ in the evaporating thin film region, the effect of the disjoining pressure diminishes to zero. In the C–C or D–D thin film region, the contact angle variation directly affects the thin film profile and the heat transfer rate through the thin film region. Although the highest heat flux is nearly the same, the total heat transfer through the thin film region increases as the contact angle decrease. As shown in Fig. 4b, the effect of contact angle on the heat flux profile and maximum heat flux can be negligible for the B–B thin film region. Comparison of the results shown in Fig. 4a with those in Fig. 4b indicates that the heat flux distributions for the B–B and C–C regions are similar. The heat fluxes for both regions are initially zero at the origin point where the film thickness is equal to δ_0, and then increase dramatically as the film

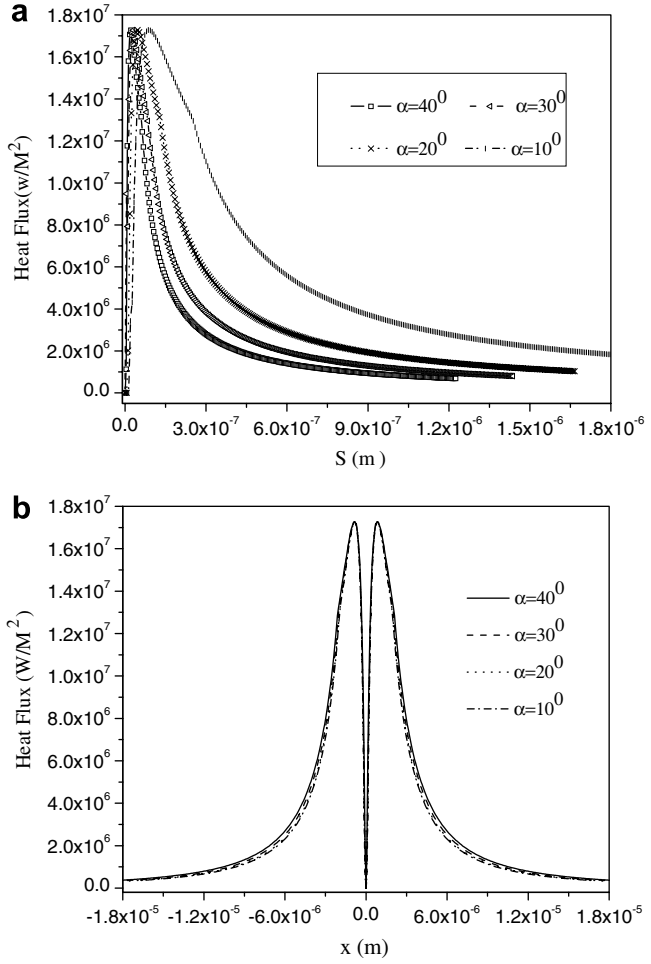

Fig. 4. Contact angle effect on heat flux distributions ($T_w - T_e = 1$ K). (a) C–C or D–D thin film region, (b) B–B thin film region.

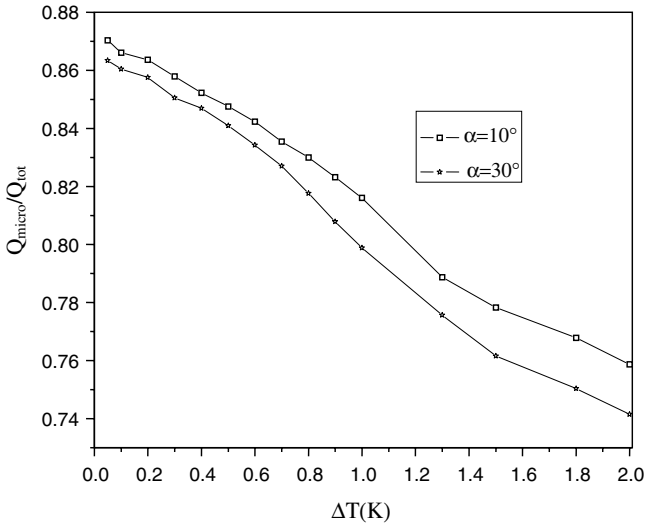

Fig. 5. Contact angle effect on Q_{micro}/Q_{tot}.

thickness increases. After reaching the maximum heat flux, the heat flux through the thin film decreases quickly along the x (or s) direction until it reaches the meniscus region.

Fig. 5 illustrates the superheat effect on the ratio of the heat transfer through the thin film region, Q_{micro}, to the total heat transfer, Q_{tot}. As shown, when the superheat increases, the ratio,Q_{micro}/Q_{tot}, decreases and it also depends on the contact angle. When the contact angle increases from 10° to 30°, for example, the ratio Q_{micro}/Q_{tot} decreases from 87.0% to 75.9% for a superheat of 2.0 K. The main reason is that the thin film region in the C–C or D–D region has been extended and heat transfer through those regions enhanced when the contact angle decrease. The temperature distribution and heat transport through the macro-region from the wall to the vapor phase can be obtained by the FLUENT software. Fig. 6 illustrates the liquid film profile and the temperature distribution in the macro-region of the liquid film. The temperature difference between two isotherms is equal to 0.05 K. As shown in this figure, the large temperature gradient existing in the thin film evaporation region creates an ultra-high heat flux and the thin film region in the B–B zone is much large than that of C–C and D–D zones.

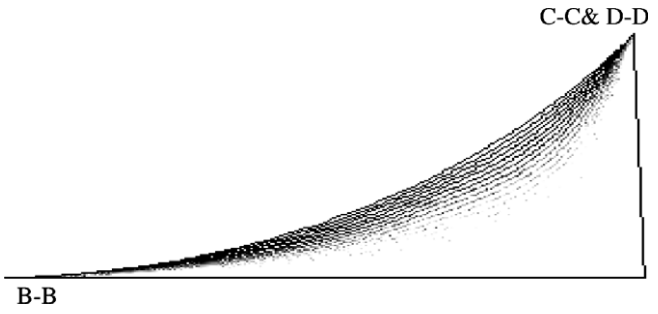

Fig. 6. Isotherms in the liquid film (temperature difference between two isotherms is 0.05 K) at $\Delta T = 1$ K.

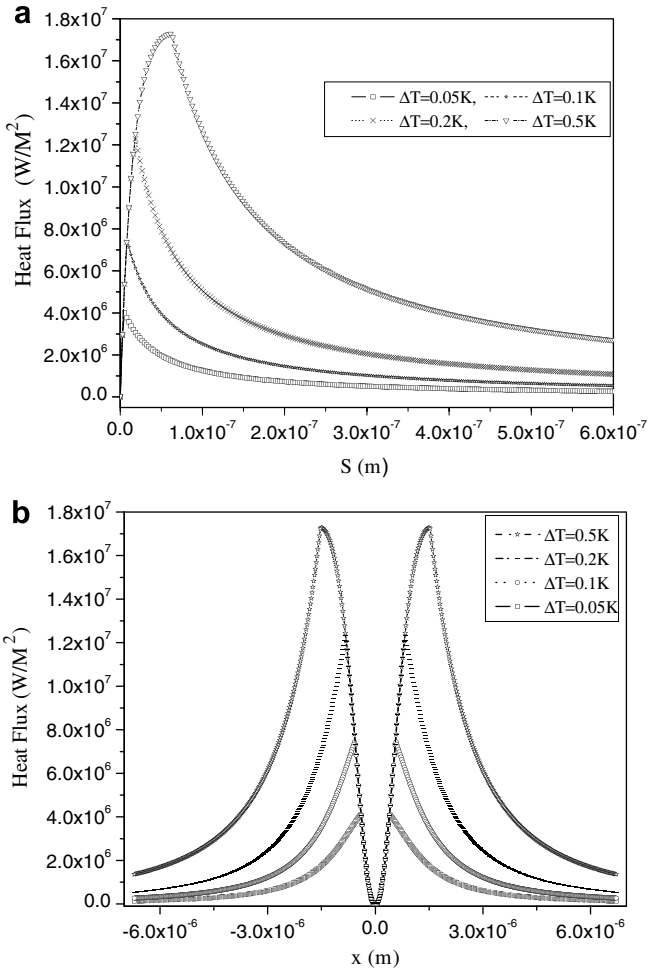

Fig. 7. Superheat and disjoining pressure effects on the heat flux distribution at $\alpha = 30°$ (a) C–C(D–D) parts, (b) B–B part.

As shown in Fig. 7a and b, the effects of superheat and disjoining pressure drop on the heat transfer in thin film evaporation are critical at the same contact angle. With the temperature difference between the groove wall and saturate vapor increases, the heat flux increases and the heat transfer through regions B–B, C–C or D–D enhances. On the other hand, the temperature difference between the wall temperature (T_w) and interface temperature T_{lv} of liquid and vapor flow, as shown in Eqs. (2) and (3), decreases due to the disjoining pressure drop effect in the thin film region. The heat flux profiles in the region from the interline to the highest heat flux directly illustrate that the disjoining pressure plays more important role in the thinner film region since thinner film thickness creates a larger disjoining pressure.

As presented above, the B–B thin film region plays an important role and the total heat transfer through this region is much larger than that through the C–C or D–D region. Therefore, the B–B thin film region should determine the total evaporating heat transfer in the evaporator, and the total effective thermal conductivity of the whole heat pipe. In addition, the contact angle has a little effect on the B–B thin film region and can be neglected. The effects of contact angle on the thin film profile and heat flux distribution for the C–C or D–D region, however, is significant.

5. Conclusions

A mathematical model predicting the meniscus radius and its effect on the thin film profile has been developed. The model includes the effects of disjoining pressure and surface tension on the interface temperature and heat flux distribution in the evaporating thin film region. The model can be used to predict the maximum heat transport capacity for a given grooved heat pipe with micro-trapezoidal grooves. The disjoining pressure effect on the thin film evaporation cannot be neglected. The results indicate that for a given superheat, $T_w - T_e$, the effect of contact angle on the thin film profile and heat flux distribution for the C–C or D–D thin film region is significant, while it can be negligible for the B–B region. For a given contact angle, the ratio of the heat transfer through the thin film region to the total heat transfer, i.e., Q_{micro}/Q_{tot}, decreases with the superheat, $T_w - T_e$. For the grooved heat pipe investigated here, the total heat transfer through the B–B thin film region is much larger than that through the C–C or D–D region, and the B–B thin film region plays an important role in determining

the maximum heat transport capability. The current investigation will result in a better understanding of thin film evaporation and its effect on the effective thermal conductivity in a grooved heat pipe and contribute to the optimization design of conventional grooved heat pipes.

References

[1] F.W. Holm, S.P. Goplen, Heat transfer in the meniscus thin film transition region, ASME J. Heat Transfer 101 (1979) 543–547.

[2] Y. Kamotani, Evaporator film coefficients of grooved heat pipe, in: Proceeding of the Third International heat Pipe Conference, Stanford Press, Palo Alto, CA, 1978, pp. 128–130.

[3] P.C. Stephan, C.A. Busse, Analysis of the heat transfer coefficient of grooved heat pipe evaporator walls, Int. J. Heat Mass Transfer 35 (1992) 383–391.

[4] A.J. Jiao, R. Riegler, H.B. Ma, G.P. Peterson, Thin film evaporation effect on heat transport capability in a groove heat pipe, J. Microfluidics Nanofluidics 1 (3) (2005) 227–233.

[5] H.B. Ma, G.P. Peterson, Temperature variation and heat transfer in triangular grooves with an evaporating film, J. Thermophys. Heat Transfer 1 (1) (1997) 90–97.

[6] P.C. Wayner, Thermal and mechanical effects in the spreading of a liquid film due to a change in the apparent finite contact angle, ASME J. Heat Transfer 117 (1994) 938–945.

[7] H.B. Ma, G.P. Peterson, Experimental investigation of the maximum heat transport in triangular grooves, ASME J. Heat Transfer 118 (1996) 740–745.

[8] S. Demsky, H.B. Ma, Thin film evaporation on a curved surface, J. Microscale Thermophys. Eng. 8 (3) (2004) 285–299.

[9] A.J. Jiao, H.B. Ma, J.K. Critser, Heat transport characteristics in miniature flat heat pipe with wire core wicks, ASME J. Heat Transfer, submitted for publication.

[10] A.J. Jiao, H.B. Ma, J.K. Critser, An investigation of heat transport capability in a miniature loop heat pipe, ASME J. Electron. Pack., submitted for publication.

[11] Y. Cao, A. Faghri, Analytical solutions of flow and heat transfer in a porous structure with partial heating and evaporation on the upper surface, Int. J. Heat Mass transfer 37 (10) (1994) 1525–1533.

[12] D. Khrustalev, A. Faghri, Thermal analysis of a micro heat pipe, Journal of Heat Transfer 116 (1) (1994) 189–198.

[13] R. Hopkins, A. Faghri, D. Khrustalev, Flat miniature heat pipes with micro capillary grooves, ASME J. Heat Transfer 121 (1) (1999) 102–109.

[14] B.R. Babin, G.P. Peterson, D. Wu, Steady state modeling and testing of micro heat pipe, ASME J. Heat Transfer 112 (1990) 595–601.

[15] S.J. Kim, J.K. Seo, K.H. Do, Analytical and experimental investigation on the operational characteristics and the thermal optimization of a miniature heat pipe with a grooved wick structure, Int. J. Heat Mass Transfer 46 (2003) 2051–2063.

[16] A. Faghri, Heat Pipe Science and Technology, Taylor and Francis, Washington, DC, 1995.

[17] G.P. Peterson, H.B. Ma, Temperature response of heat transport in a micro heat pipe, ASME J. Heat Transfer 121 (1999) 438–445.

[18] X. Xu, Y.P. Carey, Film evaporation from a micro-grooved surface-an approximate heat transfer model and its comparison with experimental data, J. Thermophys. Heat Transfer 4 (1990) 512–520.